PREDICTING OF DYNAMIC PERFORMANCES OF HELICOPTER THREE-SHAFT GAS TURBINE

G. Crosa, G. Ferrari, G. Pezzuto, M. Troilo, A. Trucco
Istituto di Macchine e Sistemi Energetici - Università di Genova
Genova - Italia

Abstract

This paper presents a numerical simulation technique for the prediction of the off-design and dynamic behaviour of an aeronautic gas turbine engine and for the realisation of the relative computational code. The mathematical model is non-linear, based on the lumped parameter approach and described by a set of first-order differential and algebraic equations. The plant components are described adding to their steady state characteristic the dynamic equations of mass and energy conservation. The state variables are the mass flow rates, the total pressures, the total temperatures of the fluid, the wall temperatures and the rotational speed of the shafts.

The model setting-up has been done on a three-shaft 700 kW gas turbine for rotorcraft application. The presented computational code is suitable to carry out a precise description of the engine actual dynamic behaviour, and is able to cover the whole operating range, also in off-design conditions. This way, the engine performances have been foreseen on the whole working range with good precision, during a transient too. The transient behaviour, in dead, is essential also as regards the optimisation of the auxiliary fittings and the control system of the gas turbine engine. Then, the comparison between the computed results and the experimental steady state data and some dynamic responses of an helicopter engine taken as example are presented to validate the proposed model.

The code works into the Simulink package (Mathworks software) and is implemented on personal computer. It allows, also, a more precise simulation of plant components introducing, into Simulink blocks, FORTRAN code describing a component or its part.

The code is useful for the engine performance improvement, being readily understandable also by people with not skilled in simulation.

List of symbols

C = component thermal capacity
C_s = brake torque
c_p = specific heat at constant pressure
c_v = specific heat at constant volume
H_i = fuel heat value
J = inertia of the rotor
K = coefficient for the heat exchange between the component internal flow and its wall
K' = coefficient for the heat exchange between the component wall and its exterior
K_{nozzle} = losses exhaust nozzle coefficient
K_{prop}, K_{int} = gains of flue flow mass PI governor
m = mass flow rate
M_{rid} = reduced mass flow
N_{HP} = high pressure rotor speed
N_{LP} = low pressure rotor speed
N_{PT} = power rotor speed
p_0 = total pressure
R = gas constant in the state equation
S = component wall surface
T_0 = total temperature
T_{0d} = dynamic total temperature
T_{amb} = air temperature
T_{rif} = reference temperature
T_w = wall temperature
V = component volume
β = compression ratio
γ = specific heat ratio ($= c_p/c_v$)
η = component efficiency
η_m = mechanical efficiency component

Abbreviations

LC = low pressure compressor
HC = high pressure compressor
LT = low pressure turbine
HT = high pressure turbine
PT = power turbine
CC = combustion chamber

Subscripts

1,2,2d,....... = cross sections referred to the plant stations as in Fig. 2
a = air
f = fuel
g = gas

The three-shaft gas turbine engine

The considered engine has been specifically designed for the helicopter propulsion. It consists of a two shafts hot-gas generator and a power turbine. The low pressure group is made up by a four-stages axial compressor, moved by a one-stage axial turbine. The high pressure group is made by a one-stage centrifugal compressor, followed by an inverted flow annular combustion chamber and by a or ɔ-stage axial turbine. The two-stages axial free turbine has a rated rotational speed of 27000 rpm.

The choice of a two-shaft hot-gas generator has been made to obtain a fast escape away from the surging line without the need of variable geometry or blow-off (Ref. 1). In fact, to have a good operating range of engine (and therefore a compression ratio to achieve the highest power), a single-shaft generator should be equipped with variable geometry vanes, with a consequent complication of the control system (Ref. 2).

A high compression ratio allows both the increase of the thermodynamic efficiency and a reduced fuel

consumption also at low rates. This is important for the helicopters equipped with more engines. In these, in fact, each engine tends to operate, on the average, only at 50% or less of the highest power, because it must be able to keep up the vehicle if another engine would break during an emergency. The design of a many-shaft hot-gas generator requires a complexity of the seals and the bearings greater than a single-shaft does. But this way a very flexible engine is obtained with a very quick response to the power demand. It is an essential characteristic for a rotorcraft application.

The mathematical model

The plant, in terms of mathematical modelling, is a multivariable, highly non-linear, stiff process and consist of a set of algebraic and time-dependent ordinary differential equations. The evolving fluid has been considered subject to mass and energy storage and also exposed to heat transfer from the wall, taking into account the metal-stored energy. The fluid is taken as a mixture of perfect gases with temperature dependent specific heats (Ref. 3, 4, 5 and 6).

Generally, the P_j performances of an energy system can be considered depending on some v_i variables:

$$P_j = f_j(v_i), j = 1,..,n_p \text{ and } i = 1,..,n_v \qquad (1)$$

where P_j is the general performance (as power, efficiency) and v_i the general variable (as rotational speed, temperature, pressure), n_p the performance number and n_v the variable number. The v_i variables are linked themselves by the physical laws that regulate the plant operation. These laws are represented as algebraic or differential equations:

$$\frac{dv_i}{dt} = f_i(v_k), i = 1,..,n_s, k = 1,..,n_v \qquad (2)$$

$$0 = g_j(v_k), j = 1,..,n_u, k = 1,..,n_v \qquad (3)$$

where n_s is the system state number and n_u the dependent variable number. It must be:

$$n_v \geq n_s + n_u. \qquad (4)$$

The value:

$$n_d = n_v - (n_s - n_u) \qquad (5)$$

is the number of the system inputs, which are the system independent variables. In this case, the meaningful engine variables are the total thermo-dynamic quantities in the sections in which the engine is divided, as showed in Fig.1, i.e. the p_{0i} pressures, the T_{0i} temperatures and the m_i mass flows.
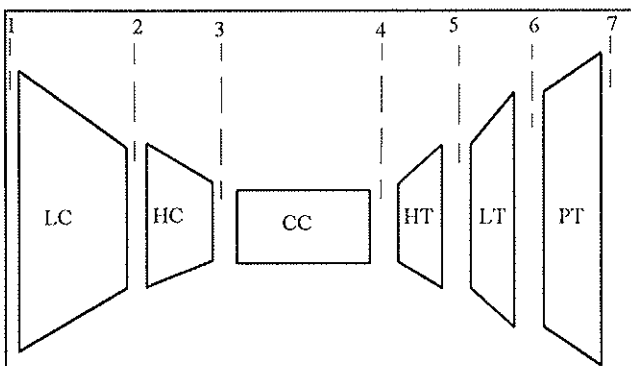
Other variables are the component wall temperatures, the rotational speeds and the brake torque.

The simulation follows the "inter-component volume" method, that assumes every block as described by the steady state component, followed by a fictitious volume where mass and energy storage takes place (Ref. 7, 8, and 9).

This way, they update the thermofluid-dynamic conditions where it is necessary to know the delay conditions in mass storage and the variation of thermodynamic quantities in each section (Ref. 10). It allows to better consider the delay of the air flow rate and pressure adjustment following a disturbance.

The model in the time domain, is shortly given as:

$$\dot{x} = f_d(x, y, u) \qquad (6)$$

$$0 = f_a(x, y, u) \qquad (7)$$

where x, y, u are respectively the state vector, the output vector and the input vector and f_d and f_a the differential and algebraic function vectors. Then, to examine the behaviour of the plant, for each component the dynamic equations of continuity and energy are written, within the hypotheses of the lumped parametric approach to describe the time evolution of the inside flow. The whole three-shaft gas turbine has been described by a set of 19 first order ordinary differential equations, which constitutes a state variable representation and it is completed by a set of 31 algebraic equations linking the state variables with all useful output variables. The whole equations set is presented in the Appendix. The input variables are the atmospheric total pressure and temperature and the brake torque. There is a PI speed governor to calculate the present fuel mass flow.

In Fig.2 and 3 the fluid flow and the steady state information diagrams of the gas turbine engine are shown.
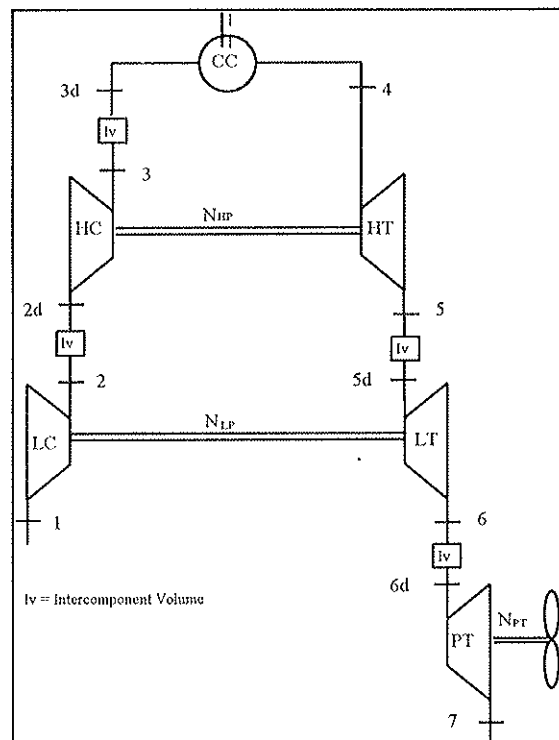

Fig.1 Engine sections numbering
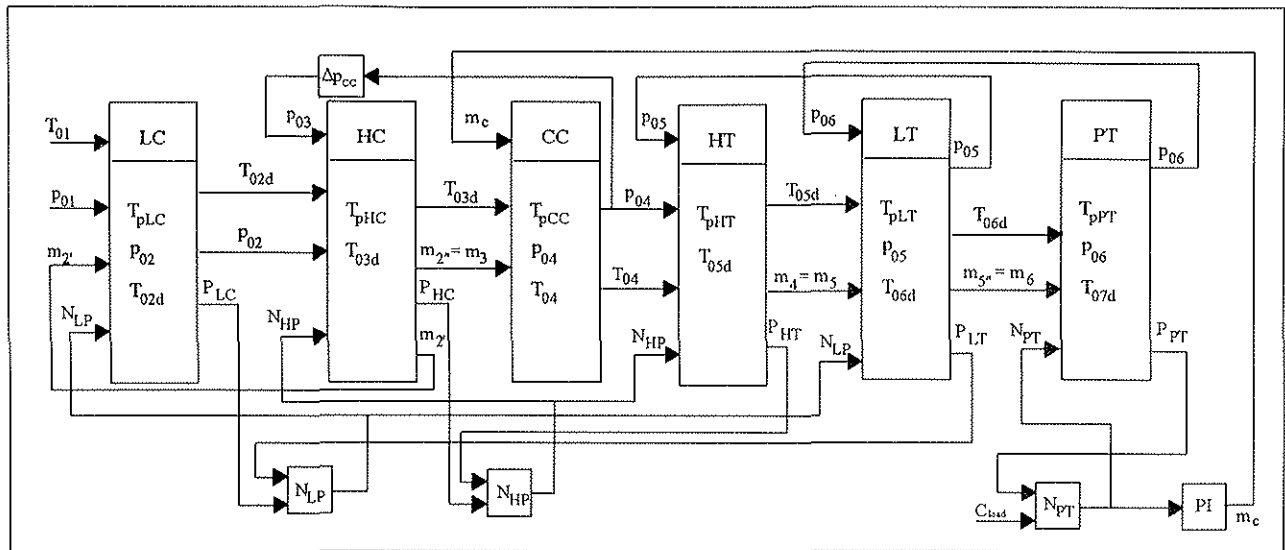

Fig.2 Plant fluid flow diagram

77.2

Fig.3 Steady-state information diagram

In the dynamic analysis every block, representative in Fig. 3 of single component, is split in two or more blocks described by first order equation in function of the time.

The energetic exchange of the bleeds with the main flow mass has not been considered because they are a small part of this.

The mechanical efficiencies are calculated as power loss: for the hot-gas generators are in function of the rotational speed; for the power turbine is function of the brake torque. The rotor inertia have been valued from the engine datasheets.

About the mathematical model, the significant plant variables have been chosen as the total thermodynamic quantities in the sections in which the engine has been separated (Fig.1). They are the pressures, the temperatures, the flows, the turbine, compressor and combustion chamber wall temperatures, the three-shaft rotational speeds and the brake torque of the free turbine. During the model formulation, some hypotheses have been made. About the wall thermal flow behaviour of every inter-component volume, the thermal capacity is considered constant as well as the temperature across the wall. The thermodynamic parameters (as the gas constant and the specific heat capacities at constant pressure and volume) are calculated with empirical correlation expressed as polynomial curves. These correlations are regarding the gas temperature and composition. The gas composition is represented by the fuel air ratio, knowing the fuel composition.

Moreover, the HC has been considered without the mass storage, then $m_3 = m_{3'}$, because a linear link exists between the p_{03} and p_{04} pressures, given by the combustion chamber pressure drop. Also, the HT mass storage has been not considered because of a link existing between the p_{07} and the external pressure given as pressure drop at the exhaust nozzle of the power turbine.

About the combustion chamber, its efficiency and pressure drop have been considered constant as a conventional value. In fact, these information are

confidential and so very difficult to get, because the efficiency and the pressure drop affect considerably the engine performance, as the presented mathematical model has shown.

Turbomachinery characteristics. To describe the HC and LC off-design steady-state behaviour, the characteristic maps of each compressor have been used, given from the engine building company as sketched curves (Ref. 11). These adiabatic efficiency and reduced mass flow curves, at several constant rotational speeds, cover the whole total pressure ratio working range. The steady-state operating points in these maps are poor, suffering from experimental uncertainties and given in a non-regular way.

Some points of each curve at constant rotational speed have been taken to have the values of reduced rotational speed, reduced mass flow, pressure ratio and efficiency in form of tabular data. During the simulation running, two subroutines (one for each compressor) are called to find, given the present values of reduced rotational speed and pressure ratio, by linear interpolation, the present values of reduced mass flow and efficiency. These subroutines have been written in 32-bit FORTRAN 77 instructions, inserted into a Simulink block as "mex-file" and properly linked to other component blocks.

The characteristics curves of the HT, LT, and PT have been obtained form experimental data. In the engine simulation, the turbine are assumed to be choked, so simple polynomial curves, independent of the rotational speed, have been taken as turbine characteristics. The efficiency of every turbine is in function of the enthalpy gradient and of the rotational speed.

The computer program

The gas turbine code runs into Simulink package on personal computer.

Simulink facilitates graphically the model definition using block diagram windows. The model is created connecting with graphical lines a succession of blocks,
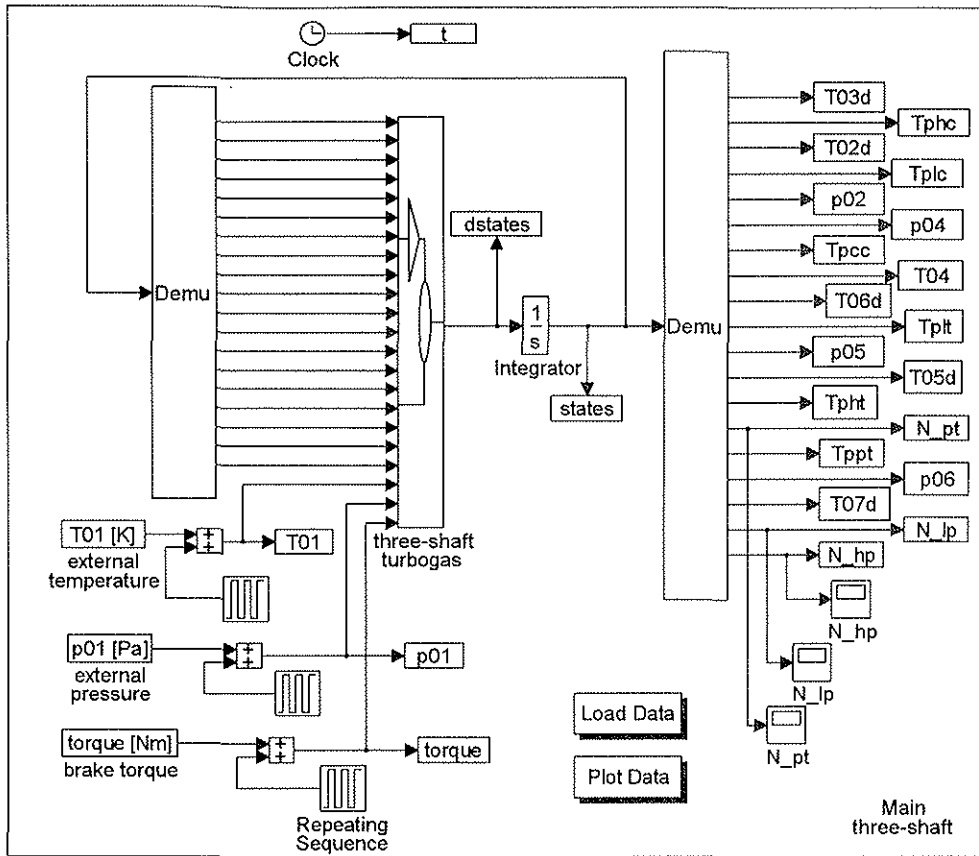
Fig.4 Simulink main layout of plant model

that can be simple block (available in library as integrator, derivative, sum or product, etc.) or more complex blocks, built by the user with Matlab language.

To reduce the model complexity some plant component can be described by Matlab program or FORTRAN code. The 32-bit MicroWay FORTRAN 77 compiler was used as recommended by the Mathworks Inc. For every FORTRAN block two interpreter blocks have to be installed to translate the FORTRAN into Simulink language, that is settled in C language environment.

mathematical model. There are other components to manage the simulator, as the integrator block to integrate the state derivative vector, the repeating sequence block to have time variable system inputs, the blocks to load the plant parameters and to plot the simulation results. In the Fig. 5, obtained by expanding the former, the main components are shown.
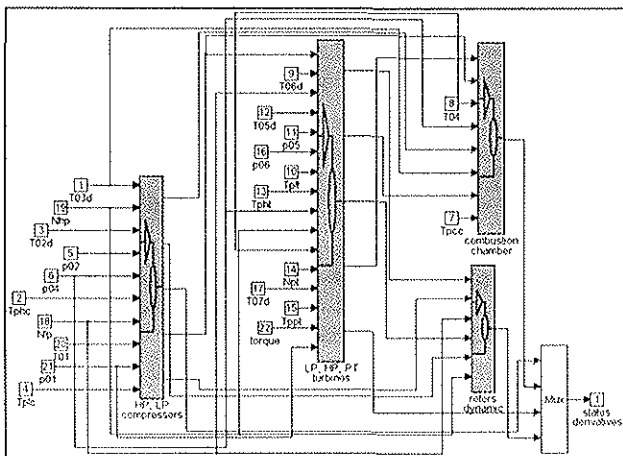
Fig.5 Three-shaft gas turbine layout
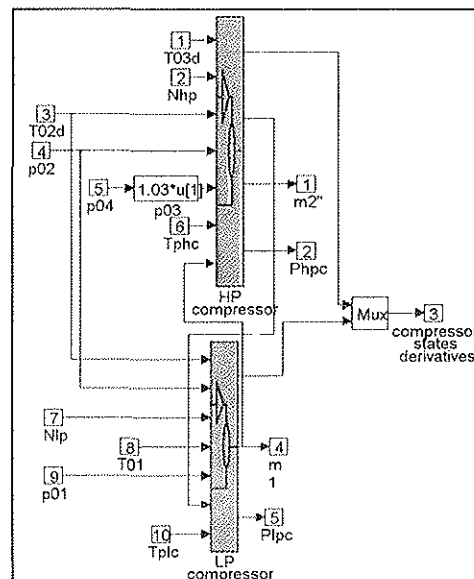
Fig.6 Further Simulink sub-scheme of compressors

Simulink block diagram. The Fig.4 shows the main layout of Simulink dynamic model. The block called "three-shaft turbogas" is including the whole

The Fig.6 is the further sub-scheme of the "HP and LP compressors" and the Fig.7 is the scheme of the "HP compressor".The Fig.8 shows the exploded of the block

called "HPC m2_p, eta_hpc", where is the block S-function which calls the subroutine FORTRAN to make the linear interpolation. The Fig.9 is obtained by expanding the "HP, LP and PT turbines" block of Fig.4, the Fig.10 is the opened block called "power turbine"; in Fig.11 the PI speed governor is shown.
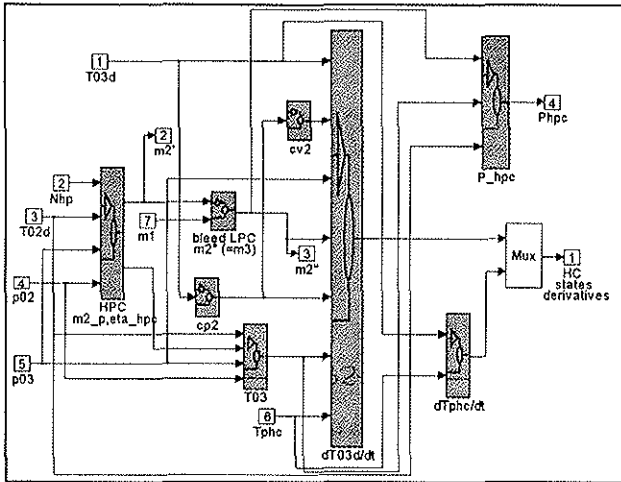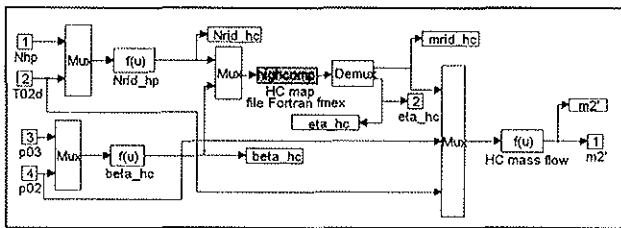

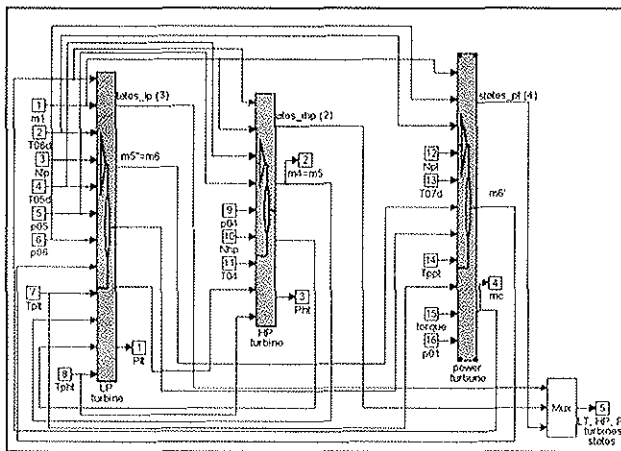**Fig.7 HC Simulink exploded**

Fig.8 HC FORTRAN mex-file block

Fig.9 Further Simulink sub-scheme of turbines

<u>**Results and discussion**</u>

The code is able to simulate fast transients and the run times are not very long: the calculation of the presented transients of the engine has required few minutes on a Pentium 90 PC.

Then, the non-linear time-dependent model is able to simulate wide load variations but the accuracy of the results depend on the validity of the data used to represent the component off-design behaviour.
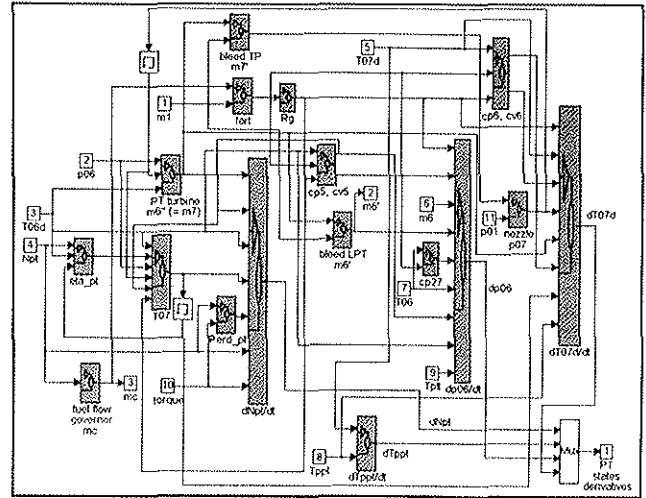

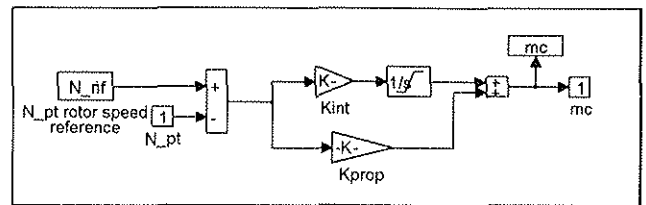**Fig.10 PT Simulink layout**

Fig.11 Simulink PI speed governor

It has not been possible to check the dynamic solution because results of dynamic tests were not available. Nevertheless, some observations and the agreement of the results comparing the dynamic computation solution with the steady-state data confirm the validity of the presented model.

In all figures, the variables are expressed as per unit (p.u.) of their value referred to the greatest efficiency conditions, indicated with apex '*'.

About the comparison between the code results and the experimental data, the steady-state solution has been checked against the manufacturer characteristic curves.

In the Figs. 12 and 13 over two compressor planes the characteristic curves are shown (as reported from the tables) together with the comparison between the experimental operating points and the simulated working line.
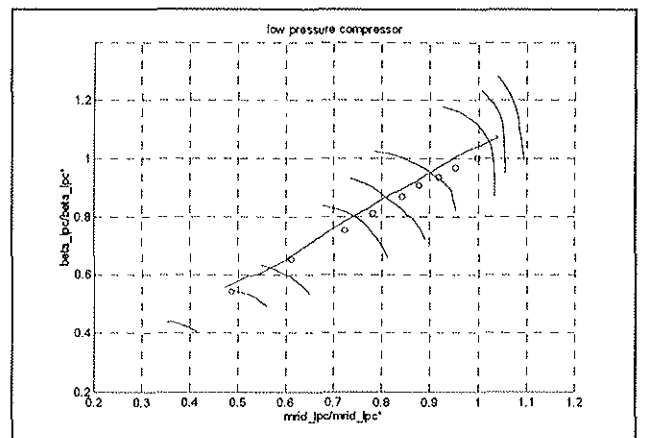

Fig.12 Comparison between operating points and working line model on LC performance map
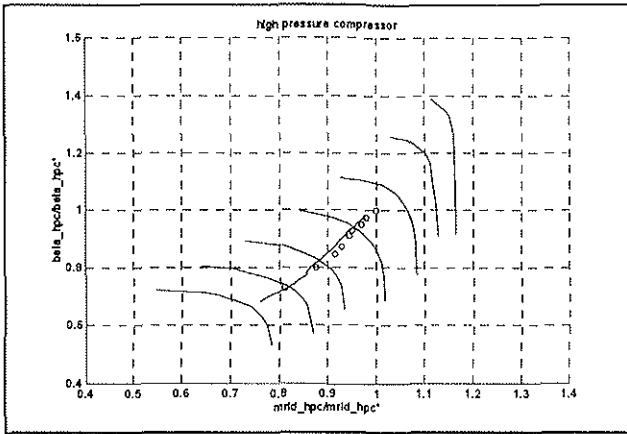
Fig.13 Comparison between operating points and working line model on HC performance map

This one has been obtained by a slow time variation of the engine brake torque from the minimum to the maximum value. In fact, Simulink finds the steady-state solution by dynamic way. The comparison seems good but it is important to validate the scientific method to foresee the engine performances, because it is always possible to improve the agreement by changing the values of the model parameters.

In the Figures from 14 to 17 the comparisons between experimental operating points and code results of the fuel mass flow, HC outlet pressure, the inlet air mass flow and the CC outlet temperature are shown.
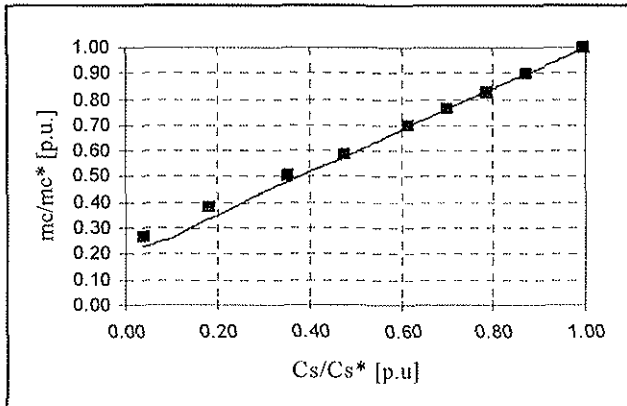

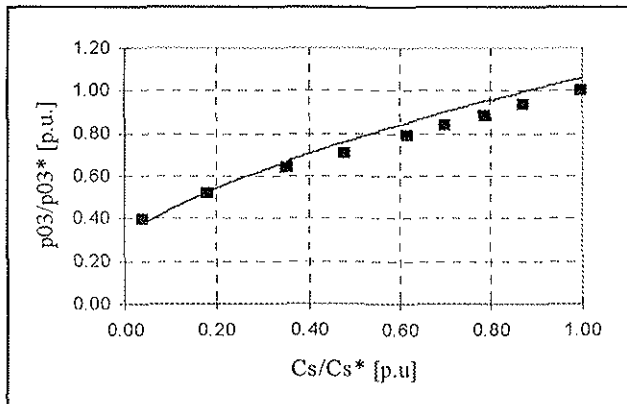**Fig.14 Fuel mass flow comparison between operating points and simulation data**

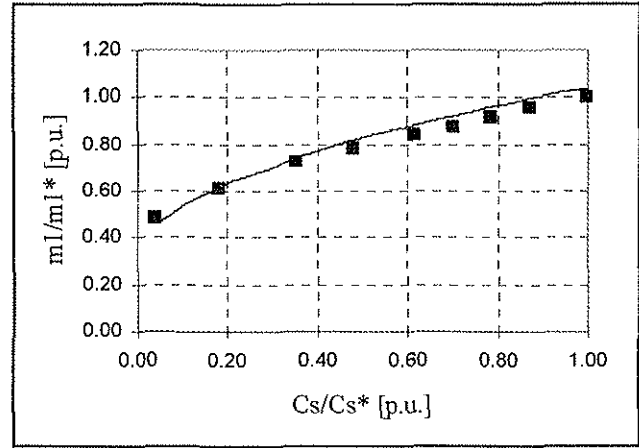**Fig.15 HC outlet pressure comparison between operating points and simulation data**

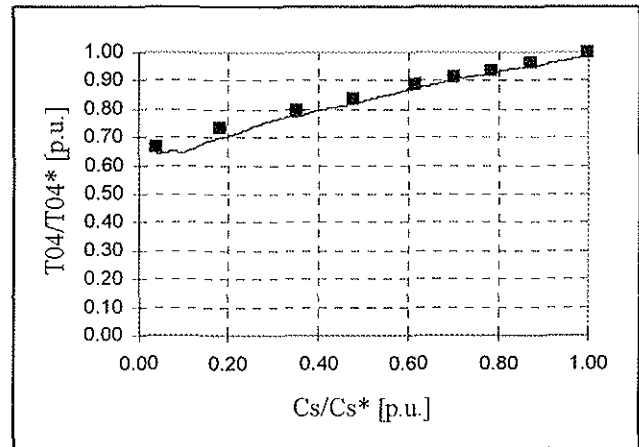**Fig.16 Inlet air mass flow comparison between operating points and simulation data**

Fig.17 CC outlet temperature comparison between operating points and simulation data

In the Figs.18 and 19 on the two compressor maps a transient trajectory by a torque schedule from 100% to 20% in 2 seconds is shown. The Figs.20 and 21 show a transient trajectory by a torque schedule from 20% to 100% in 3 seconds.
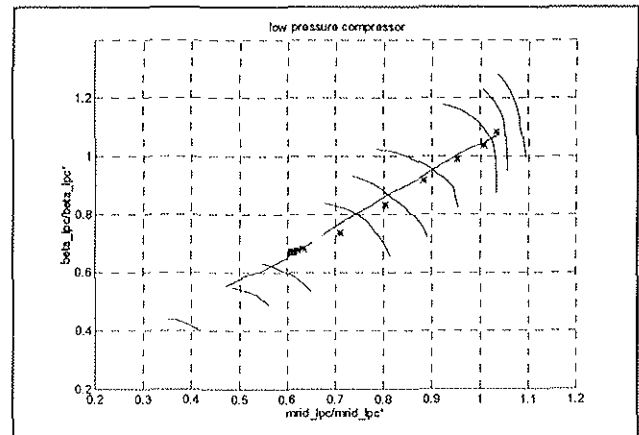

Fig.18 Transient trajectory on LC map by a torque schedule from 100% to 20% in 2 seconds

Of course, during the first instants of the transient, there is a shifting of the trajectory from the static working line (Ref. 12 and 13). In particular, the

behaviour of the dynamic curve on the LC map is in disagreement with the theory, because this dynamic curve is moving, as regards the working line, in the same way as the HC.
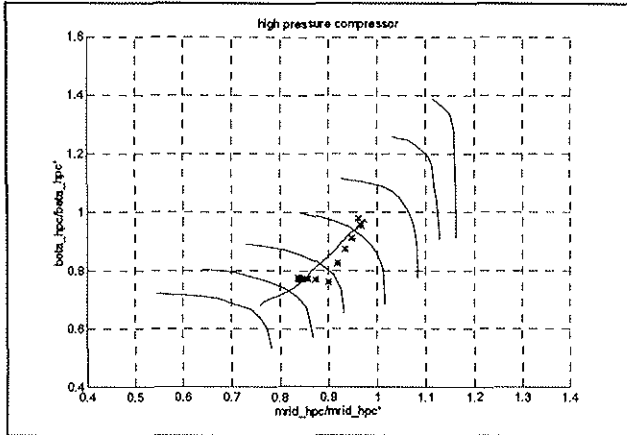

Fig.19 Transient trajectory on HC map by a torque schedule from 100% to 20% in 2 seconds
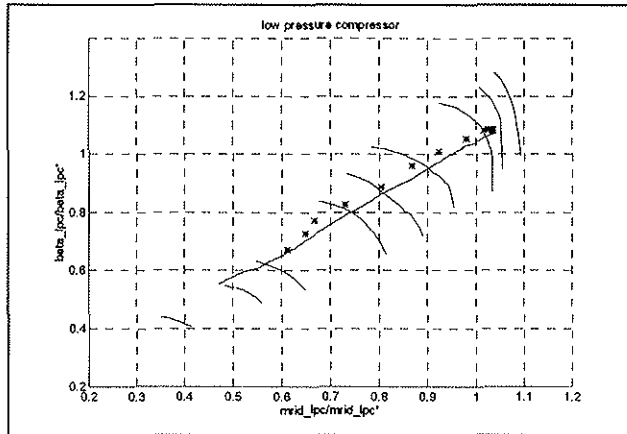

Fig.20 Transient trajectory on LC map by a torque schedule from 20% to 100% in 3 seconds
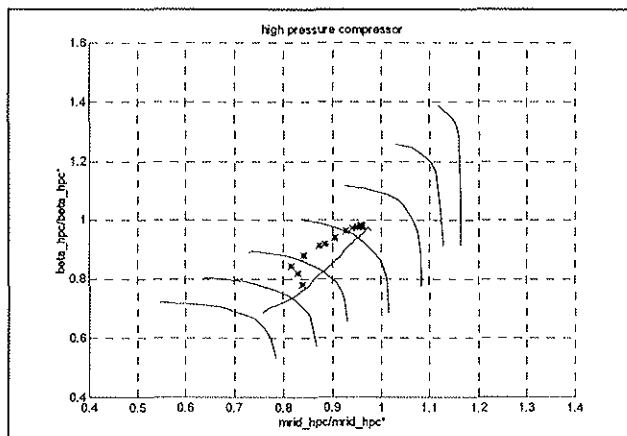

Fig.21 Transient trajectory on HC map by a torque schedule from 20% to 100% in 3 seconds

In the Figures from 22 to 29 the transient plots of the most important parameters of the plant, connected with a torque schedule, are shown. Starting from a steady-state conditions at 60% of rated torque, at 5 seconds of simulation time, a ramp of +30% is imposed in 0.5 seconds (Fig.22).
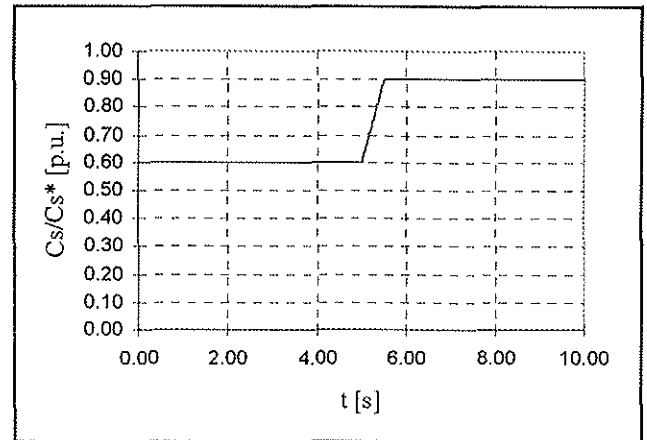

Fig.22 Torque ramp from 60% to 90% in 0.5 seconds

In the Figs.23 and 24 the transient trajectory on the respective LC and HC maps is shown.
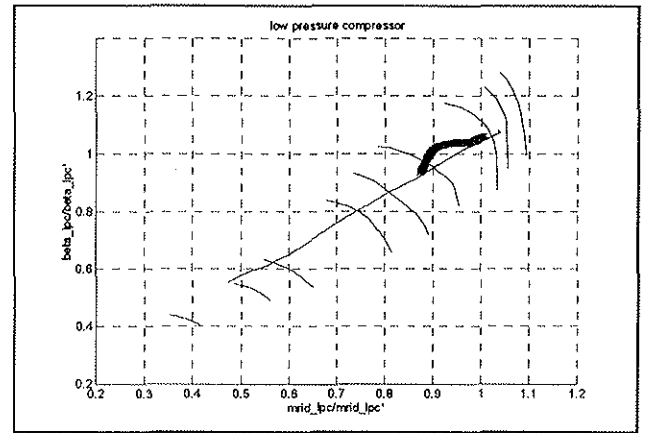

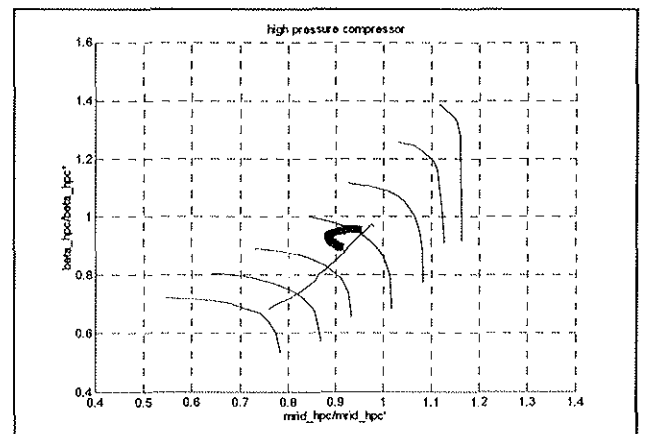**Fig.23 Transient trajectory on LC map by a torque ramp from 60% to 90% in 0.5 seconds**

Fig.24 Transient trajectory on HC map by a torque ramp from 60% to 90% in 0.5 seconds

The Fig.25 shows the fuel mass flow, during the first instants, is increasing how over than the final steady-state value, to supply the considerable energy required to

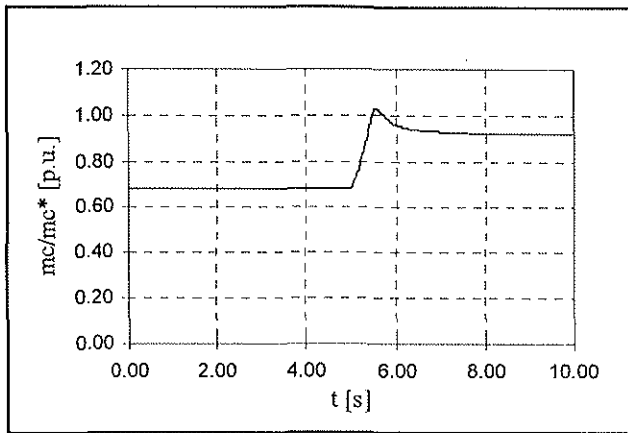accelerate the high and low pressure hot-gas generator groups.

Fig.25 Transient plot of fuel mass flow by a torque ramp from 60% to 90% in 0.5 seconds.

In fact, the increase of the fuel flow rate must quickly make up for the unavoidable decrease of the PT shaft rotational speed, that is depending on its controller.

Because the hot-gas generator groups accelerate with sensible delay (Fig.26), the air mass flow is slowly increasing (Fig.27) and the plant greatest temperature has an overshoot (Fig.28), which could be dangerous without a temperature limiter.
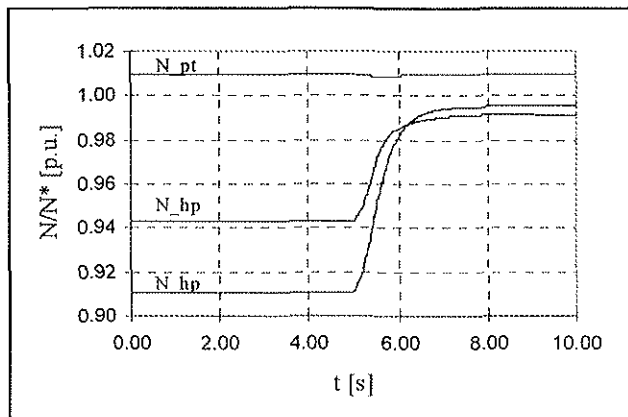

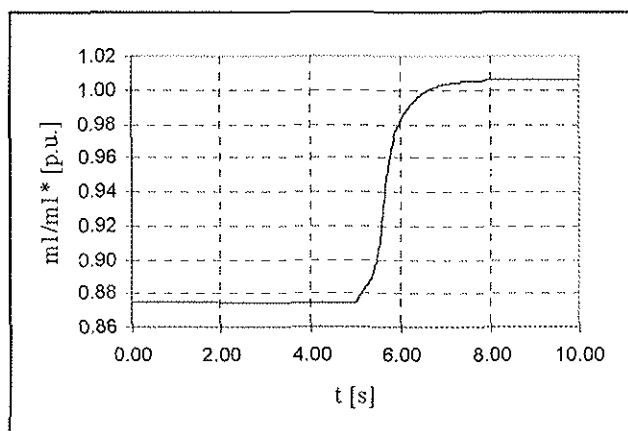**Fig.26 Transient plot of shaft rotational speed by a torque ramp from 60% to 90% in 0.5 seconds.**

Fig.27 Transient plot of inlet air mass flow by a torque ramp from 60% to 90% in 0.5 seconds.
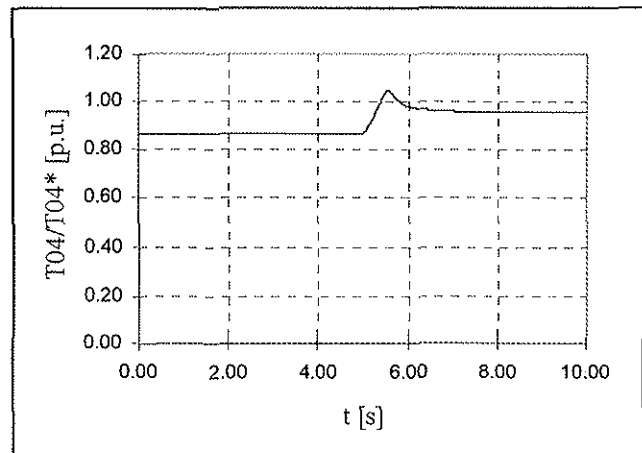

Fig.28 Transient plot of CC outlet temperature by a torque ramp from 60% to 90% in 0.5 seconds.

Then, the increasing of the air mass flow and the HC outlet pressure (Fig.29), due to groups rotational speed raise, reduces the fuel flow demand.
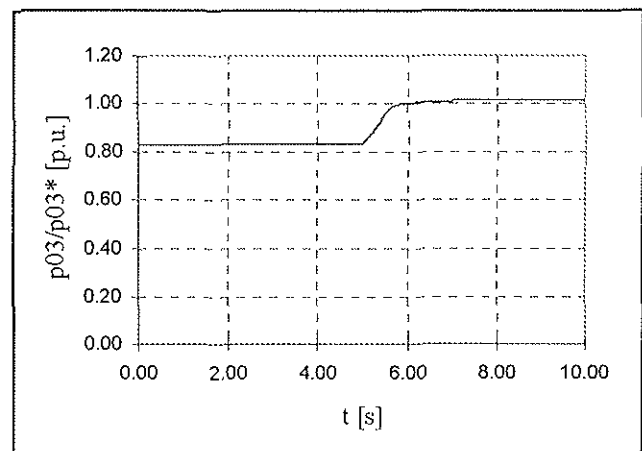
Fig.29 Transient plot of HC outlet pressure by a torque ramp from 60% to 90% in 0.5 seconds.

To keep constant the shaft PT rotational speed at a reference speed, the fuel mass flow is governed by a PI speed controller. A future research will examine the governor setting-up to obtain optimum conditions during the gas turbine engine control, to keep constant the rotational speed of the power turbine and to avoid the burn out (Ref. 14).

Conclusion

A dynamic gas turbine simulation program has been realised. The code is not simple, in spite of the effort done to avoid superfluous information. To study fast transients, the characteristic maps of turbomachines have to be effective in a large range of operation and it is not easy to obtain. However, in the steady-state range, near the design point, the accuracy is very important, besides there are regions where calculations could only show the general behaviour of the plants. For instance, during the acceleration of a gas turbine engine, the compressors can pass through the rotating stall region and even the mass flow rate could reverse. The stall and

the surge characteristics of the compressor are generally not well known but the simulation can give important information for a safe design of gas turbine engine.

The code seems to reflect accurately the performance of the corresponding actual plant so that designers can test the impact of component changes or malfunctions on the cycle efficiency.

The code is modular and component models can be easily replaced; it is only necessary to comply with the input and output variables. Different power and architecture can be analysed without problems. The model will be improved by adding a whole fuel control system and extending the range of machine characteristics to simulate start-up and shut-down transient.

REFERENCES

1. H. Wittemberg, *Prediction of Off-design Performances of Turbojet and Turbofan Engine*, AGARD-CP 242, 1977
2. A.J. Fawke, H.I.H. Saravanamuttoo, *Experimental Investigation of Methods for Improving the Dynamic Response of a Twin-Spool Turbojet Engine*, Trans. ASME 418, Oct. 1971
3. B.D. MacIsacc, H.I.H. Saravanamuttoo, *An Overview of Engine Dynamic response and Mathematical Modelling Concepts*, AGARD-CP 224
4. E.B. Mats, A.P. Tunakov, *Requirements on modern Mathematical Models of Gas Turbine Engines. Part 1*, Izvestiya VUP Aviatsionnaya Tekhnika, Vol.24, No 1, 1981
5. E.B. Mats, A.P. Tunakov, *Requirements on modern Mathematical Models of Gas Turbine Engines. Part 2*, Izvestiya VUP Aviatsionnaya Tekhnika, Vol.25, No 3, 1982
6. A.P. Tunakov, *Classification of Gas Turbine Engine Mathematical Models*, Izvestiya VUP Aviatsionnaya Tekhnika, Vol.29, No 4, 1981
7. H. Cohen, G.F.C. Rogers, H.I.H. Saravanamuttoo, *Gas Turbine Theory*, Longman Scientific & Technical
8. A.J. Fawke, H.I.H. Saravanamuttoo, *Digital Computer Methods for Prediction of Gas Turbine Dynamic Response*, SAE 710550
9. J. Seller, F.Teren, *Generalised Dynamic Engine Simulation Techniques for the Digital Computer*, AGARD-CP 151, 1974
10. S.E. Aksellrod, V.M. Kofman, *A Criterial Approach to Evaluation of Working Fluid Mass and Energy Accumulation in Volumes of the Gas Turbine Engine Flow section in calculation of Non-Steady Regimes*, Izvestiya VUP Aviatsionnaya Tekhnika, Vol.26, No 1, 1983
11. A.J. Fawke, M. Holmes, H.I.H. Saravanamuttoo, *Experimental Verification of a Digital Computer Simulation Method for Predicting Gas Turbine Dynamic Behaviour*, Proc. Inst. Mech. Eng. 1972
12. B. Thomson, *Basic Transient Effects of Aero gas Turbine*, AGARD-CP 242, 1977
13. M.R. Maltby, *Acceleration Performance of Helicopter Engines*, Trans. ASME Journ. of Eng. for Gas Turbine and Power, Vol. 109, April 1987
14. T.H. Wong, *Designing and Simulating the Engine Speed Governor for Helicopter Applications*, ASME Paper, 95-GT-158

APPENDIX

The whole equation set of the three-shaft gas turbine is described by the following equations.

Set of differential equations:

- LC volume energy storage equation:

$$\frac{\partial T_{02d}}{\partial t} = \frac{R_a T_{02d}}{c_{v1} p_{02} V_{LC}} [m_2 c_{p12}(T_{02} - T_{rif}) - m_2 c_{p1}(T_{02d} - T_{rif}) + - K_{LC} S_{LC}(T_{02d} - T_{pLC}) + c_{v1}(T_{02d} - T_{rif})(m_2 - m_{2'})]$$

(A1)

- HC volume energy storage equation:

$$\frac{\partial T_{03d}}{\partial t} = \frac{R_a T_{03d}}{c_{v2} p_{03} V_{HC}} [m_3 c_{p2}(T_{03} - T_{03d}) - K_{HC} S_{HC}(T_{03d} - T_{pHC})]$$

(A2)

- CC volume energy storage equation (this equation includes the HT equivalent volume):

$$\frac{\partial T_{04}}{\partial t} = \frac{R_g T_{04}}{c_{v3} p_{04} V_{CC}} [m_{3'} c_{p2}(T_{03d} - T_{rif}) - m_4 c_{p3}(T_{04} - T_{rif}) + m_c H_i \eta_{CC} K_{CC} S_{CC}(T_{04} - T_{pCC}) - c_{v3}(T_{04} - T_{rif})(m_4 - m_c - m_{3'})]$$

(A3)

- HT volume energy storage equation:

$$\frac{\partial T_{05d}}{\partial t} = \frac{R_g T_{05d}}{c_{v4} p_{05} V_{HT}} [m_5 c_{p45}(T_{05} - T_{rif}) - m_5 c_{p4}(T_{05d} - T_{rif}) + - K_{HT} S_{HT}(T_{05d} - T_{pHT}) - c_{v4}(T_{05d} - T_{rif})(m_5 - m_{5'})]$$

(A4)

- LT volume energy storage equation:

$$\frac{\partial T_{06d}}{\partial t} = \frac{R_g T_{06d}}{c_{v5} p_{06} V_{LT}} [m_6 c_{p56}(T_{06} - T_{rif}) - m_6 c_{p5}(T_{06d} - T_{rif}) + - K_{LT} S_{LT}(T_{06d} - T_{pLT}) - c_{v5}(T_{06d} - T_{rif})(m_6 - m_{6'})]$$

(A5)

- PT volume energy storage equation:

$$\frac{\partial T_{07d}}{\partial t} = \frac{R_g T_{07d}}{c_{v6} p_{07} V_{PT}} [m_7 c_{p6}(T_{07} - T_{07d}) - K_{PT} S_{PT}(T_{07d} - T_{pPT})]$$

(A6)

- LC wall heat storage equation:

$$\frac{\partial C_{LC} T_{pLC}}{\partial t} = [K_{LC} S_{LC}(T_{02d} - T_{pLC}) - K'_{LC} S_{LC}(T_{pLC} - T_{amb})]$$

(A7)

- LT wall heat storage equation:

$$\frac{\partial C_{LT} T_{pLT}}{\partial t} = [K_{LT} S_{LT}(T_{06d} - T_{pLT}) - K'_{LT} S_{LT}(T_{pLT} - T_{amb})]$$

(A8)

- HC wall heat storage equation:

$$\frac{\partial C_{HC} T_{pHC}}{\partial t} = [K_{HC} S_{HC}(T_{03d} - T_{pHC}) - K'_{HC} S_{HC}(T_{pHC} - T_{amb})]$$

(A9)

- HT wall heat storage equation:

$$\frac{\partial C_{HT}T_{pHT}}{\partial t} = [K_{HT}S_{HT}(T_{05d} - T_{pHT}) - K'_{HT}S_{HT}(T_{pHT} - T_{amb})] \tag{A10}$$

- CC wall heat storage equation:

$$\frac{\partial C_{CC}T_{pCC}}{\partial t} = [K_{CC}S_{CC}(T_{04} - T_{pCC}) - K'_{CC}S_{CC}(T_{pCC} - T_{amb})] \tag{A11}$$

- PT wall heat storage equation:

$$\frac{\partial C_{PT}T_{pPT}}{\partial t} = [K_{PT}S_{PT}(T_{07d} - T_{pPT}) - K'_{PT}S_{PT}(T_{pPT} - T_{amb})] \tag{A12}$$

- Low pressure rotor dynamic equation:

$$\frac{\partial N_{LP}}{\partial t} = \frac{1}{J_{LP}N_{LP}}[\eta_{mLP}m_5 c_{p4}(T_{05d} - T_{06}) - m_1 c_{p12}(T_{02} - T_{01})] \tag{A13}$$

- High pressure rotor dynamic equation:

$$\frac{\partial N_{HP}}{\partial t} = \frac{1}{J_{HP}N_{HP}}[\eta_{mHP}m_4 c_{p3}(T_{04} - T_{05}) - m_2 c_{p23}(T_{03} - T_{02d})] \tag{A14}$$

- Power rotor dynamic equation:

$$\frac{\partial N_{PT}}{\partial t} = \frac{1}{J_{PT}N_{PT}}[\eta_{mPT}m_6 c_{p5}(T_{06d} - T_{07}) - C_s N_{PT}] \tag{A15}$$

- LC volume mass storage equation:

$$\frac{\partial p_{02}}{\partial t} = \frac{R_a}{c_{v1}V_{LC}}[m_2 c_{p12}(T_{02} - T_{rif}) - m_{2'} c_{p1}(T_{02d} - T_{rif}) + \\ - K_{LC}S_{LC}(T_{02d} - T_{pLC}) + c_{v1}T_{rif}(m_2 - m_{2'})] \tag{A16}$$

- HC, HT and CC volume mass storage equation:

$$\frac{\partial p_{04}}{\partial t} = \frac{R_g}{c_{v3}V_{CC}}[m_{3''}c_{p2}(T_{03d} - T_{rif}) - m_4 c_{p3}(T_{04} - T_{rif}) + m_c H_i \eta_{CC} + \\ - K_{CC}S_{CC}(T_{04} - T_{pCC}) + c_{v3}T_{rif}(m_{3''} + m_c - m_4)] \tag{A17}$$

- HT volume mass storage equation:

$$\frac{\partial p_{05}}{\partial t} = \frac{R_g}{c_{v4}V_{HT}}[m_5 c_{p45}(T_{05} - T_{rif}) - m_{5'}c_{p4}(T_{05d} - T_{rif}) + \\ - K_{HT}S_{HT}(T_{05d} - T_{pHT}) + c_{v4}T_{rif}(m_5 - m_{5'})] \tag{A18}$$

- PT volume mass storage equation:

$$\frac{\partial p_{06}}{\partial t} = \frac{R_g}{c_{v5}V_{LT}}[m_6 c_{p56}(T_{06} - T_{rif}) - m_{6'}c_{p5}(T_{06d} - T_{rif}) + \\ - K_{LT}S_{LT}(T_{06d} - T_{pLT}) + c_{v5}T_{rif}(m_6 - m_{6'})] \tag{A19}$$

Set of algebraic equations:

- LC bleed:
$$m_{2''} = m_{2'} - 0.022m_1 \tag{A20}$$
- HC bleed:
$$m_{3''} = m_{3'} - 0.0307m_1 \tag{A21}$$
- HT bleed:
$$m_{5''} = m_{5'} - 0.022m_1 \tag{A22}$$
- LT bleed:
$$m_{6''} = m_{6'} - 0.022m_1 \tag{A23}$$
- PT bleed:
$$m_{7''} = m_{7'} - 0.022m_1 \tag{A24}$$

- PT thermodynamic expansion equation:

$$\frac{T_{07}}{T_{06d}} = 1 - \eta_{PT}\left[1 - \left(\frac{p_{06}}{p_{07}}\right)^{-\frac{k-1}{k}}\right] \tag{A25}$$

- HT thermodynamic expansion equation:

$$\frac{T_{05}}{T_{04}} = 1 - \eta_{HT}\left[1 - \left(\frac{p_{04}}{p_{05}}\right)^{-\frac{k-1}{k}}\right] \tag{A26}$$

- LT thermodynamic expansion equation:

$$\frac{T_{06}}{T_{05d}} = 1 - \eta_{LT}\left[1 - \left(\frac{p_{05}}{p_{06}}\right)^{-\frac{k-1}{k}}\right] \tag{A27}$$

- HC thermodynamic compression equation:

$$\frac{T_{02}}{T_{01}} = 1 + \frac{1}{\eta_{HC}}\left[\left(\frac{p_{02}}{p_{01}}\right)^{\frac{k-1}{k}} - 1\right] \tag{A28}$$

- LC thermodynamic compression equation:

$$\frac{T_{03}}{T_{02d}} = 1 + \frac{1}{\eta_{LC}}\left[\left(\frac{p_{03}}{p_{02}}\right)^{\frac{k-1}{k}} - 1\right] \tag{A29}$$

- HT efficiency (HT map):

$$\eta_{HT} = F_{HT}\left(\frac{N_{HP}}{\sqrt{T_{04} - T_{05}}}\right) \tag{A30}$$

- LT efficiency (LT map):

$$\eta_{LT} = F_{LT}\left(\frac{N_{LP}}{\sqrt{T_{05d} - T_{06}}}\right) \tag{A31}$$

- PT efficiency (PT map):

$$\eta_{PT} = F_{PT}\left(\frac{N_{PT}}{\sqrt{T_{06d} - T_{07}}}\right) \tag{A32}$$

- HC reduced mass flow and efficiency:

$$\beta = \frac{p_{03}}{p_{02}} \tag{A33}$$

$$N_{ridHP} = \frac{N_{HP}}{\sqrt{T_{02d}}} \tag{A34}$$

from the compressor map, we can find M_{ridHC} and η_{HC}; then

$$m_{2'} = M_{ridHC}\frac{p_{02}}{\sqrt{T_{02d}}} \tag{A35}$$

- LC reduced mass flow and efficiency:

$$\beta = \frac{p_{02}}{p_{01}} \tag{A36}$$

$$N_{ridLP} = \frac{N_{LP}}{\sqrt{T_{01}}} \tag{A37}$$

from the compressor map, we can find M_{ridLC} and η_{LC}; then

$$m_1 = M_{ridLC}\frac{p_{01}}{\sqrt{T_{01}}} \tag{A38}$$

- HT mass flow (HT map):

$$\frac{m_4 \sqrt{T_{04}}}{p_{04}} = G_{HT}(\beta_{HT})$$ (A39)

- LT mass flow (LT map):

$$\frac{m_{5''} \sqrt{T_{05d}}}{p_{05}} = G_{LT}(\beta_{LT})$$ (A40)

- PT mass flow (PT map):

$$\frac{m_{6''} \sqrt{T_{06d}}}{p_{06}} = G_{PT}(\beta_{PT})$$ (A41)

- Exhaust nozzle equation:

$$p_{07} = p_{01} + (m_{7''})^2 K_{nozzle}$$ (A42)

- Fuel flow PI governor equation:

$$m_c = \left(k_{prop} + \frac{k_{int}}{s}\right)(N_{rif} - N_{PT})$$ (A43)

- LC continuity equation:
  $$m_1 = m_2$$ (A44)
- HC continuity equation:
  $$m_{2''} = m_3$$ (A45)
- HT continuity equation:
  $$m_4 = m_5$$ (A46)
- LT continuity equation:
  $$m_{5''} = m_6$$ (A47)
- PT continuity equation:
  $$m_{6''} = m_7$$ (A48)
- Intercomponent volume hypotheses:
  $$m_3 = m_{3'}$$ (A49)
  $$p_{04} = 0.97 p_{03}$$ (A50)